



PREDICTION OF WELDING BEAD GEOMETRY FOR WIRE ARC ADDITIVE MANUFACTURING OF SS308L WALLS USING RESPONSE SURFACE METHODOLOGY

Van Thao Le*, Dinh Si Mai, Tat Khoa Doan, Quang Huy Hoang

Le Quy Don Technical University, No. 236 Hoang Quoc Viet Street, Hanoi, Vietnam.

ARTICLE INFO

TYPE: Research Article

Received: 21/4/2020

Revised: 19/5/2020

Accepted: 20/5/2020

Published online: 28/5/2020

<https://doi.org/10.25073/tcsj.71.4.11>

* Corresponding author.

Email: thaomta@gmail.com

Abstract. In the wire arc additive manufacturing (WAAM) process, the geometry of single welding beads has significant effects on the stability process and the final quality and shape of manufactured parts. In this paper, the geometry of single welding beads of 308L stainless steel was predicted as functions of process parameters (i.e. welding current I , voltage U , and travel speed v) by using the response surface methodology (RSM). A set of experimental runs was carried out by using the Box-Behnken design method. The adequacy of the developed models was assessed by using an analysis of variance (ANOVA). The results indicate that the RSM allows the predictive models of bead width (BW) and bead height (BH) to be developed with a high accuracy: R^2 -values of BW and BH are 99.01% and 99.61%, respectively. The errors between the predicted and experimental values for the confirmatory experiments are also lower than 5% that again confirms the adequacy of the developed models. These developed models can efficiently be used to predict the desirable geometry of welding beads for the adaptive slicing principle in WAAM.

Keywords: Wire arc additive manufacturing, gas metal arc welding, welding bead geometry, response surface methodology, ANOVA.

1. INTRODUCTION

Additive manufacturing (AM), also known as 3D printing, has largely investigated in the last four decades because of its ability of building complex components by adding materials layer-by-layer [1]. In comparison to traditional manufacturing processes (e.g. casting and machining), AM has the advantages of design freedom, reducing material wastes and environmental impacts [2,3]. AM technologies - particularly metallic AM, have been efficiently applied in different industrial sectors, for example aerospace, automotive, and biomedical engineering [1].

The metallic AM technologies can be classified into three main groups: laser-based, electron beam-based and arc welding-based AM [4]. Among them, wire arc additive manufacturing (WAAM) uses the electrical arc as the heat source to melt metallic wire and produces the parts layer-by-layer. This technique reveals high deposition rate of materials and low costs of production and investment [5]. The deposition rate of materials in WAAM can reach up to 8 kg/h, while that of laser-based and electron beam-based AM is around 0.1 - 0.2 kg/h [6]. Moreover, this technology features a high efficiency of material utilization. The use of metal wire as the feedstock material is also safer than the metal in powder form for the health of operators and environment.

The heat source used in WAAM can be gas metal arc welding (GMAW), gas tungsten arc welding (GTAW), and plasma arc welding (PAW) [7]. During GTAW-AM and PAW-AM processes, the arc is ignited between the tungsten electrode and the workpiece and the melted wire is fed into the molten pool, separately. On the other hand, the welding arc of GMAW-AM processes is directly ignited between the consumable wire and the workpiece. Thus, the wire is melted more quickly under the effect of the electric arc and the shielding gas flow. The deposition rate of GMAW-AM is generally from two to three times higher than that of GTAW-AM and PAW-AM processes [8]. Therefore, the GMAW-AM is usually used for producing components with large scale dimensions.

In comparison to the traditional welding process, in which some factors related to the welding beads such as the aspect factor or the form factor, the depth of penetration, and the bead width are usually taken in consideration [9–11], the bead width and the bead height of single welding beads play very important role in the WAAM process. They significantly influences the process stability, the final geometry and quality of manufactured parts, especially in the cases of building thin-wall components [12]. The geometry and quality of welding beads are generally controlled by the welding process parameters, such as the welding current, the arc voltage, and the travel speed. Previously published studies generally carried out a number of trial runs with different sets of process parameters to observe the geometry and quality of welding beads, and subsequently select a reasonable one for the build of components [13–15]. Other studies selected the process parameters according to the recommendation of the wire manufacturers for specified wire materials and welding conditions [16]. In addition, most of previous studies focused on exploring the manufacture of low-carbon steels [16,17] and some austenite stainless steels (e.g. 304, 304L, and 316L) [16–20] by the WAAM process. Until now, very limited studies have reported in the build of WAAM SS308L components.

Therefore, this study aims at developing the predictive models of welding beads and welding height by using the response surface methodology (RSM) for the build of thin-walled SS308L components by GMAW-AM. Based on the predictive models, the effect of main

process parameters on the geometry of welding beads can be analyzed, and the designer and process planners can predict optimal process parameters, which ensure the process stability and final quality of components built by the WAAM process.

2. MATERIALS AND EXPERIMENTAL PROCEDURE

2.1. Materials

In the experiments, a commercial 308L stainless steel wire with a diameter of 1 mm was used as the feedstock material. A number of SS400 steel plates with dimensions of 250 mm x 150 mm x 10 mm were used as the substrates in the welding process. The chemical composition of the wire and the substrate are given in Table 1.

A robotic GMAW system (Panasonic TA1400) shown in Fig. 1a was used to build all samples. During the welding process, a gas of 99.99% argon with a constant flow rate of 15 (L/min) was applied for the shielding.

Table 1. Chemical compositions of SS308L and SS400 (in wt. %).

Material	C	P	S	Si	Mn	Mo	Cu	Cr	Ni	Fe
308L wire	0.03 max	0.03 max	0.03 max	0.30- 0.65	1.0- 2.5	0.50 max	0.75 max	19.5- 21	9.0- 11.0	Bal.
SS400	0.05	0.013	0.002	0.037	0.46	-	-	-	-	Bal.

2.2. Experimental procedure

In order to develop the predictive models of the bead width and the bead height as functions of main process parameters, including the welding current I , the voltage U , and the travel speed v , a series of trial runs were designed by using the Box-Behnken method. Three levels of values were selected and coded for each factor (i.e. I , U and v), as shown in Table 2.

The limits of each parameter were chosen based on the recommendation of the wire manufacturer. These values were also verified by several trial runs to ensure the weldability and to avoid the interruption of the experiment.

Table 2. Process parameters and their levels.

Parameters	Code	Levels		
		-1	0	+1
Welding current, I (A)	A	100	120	140
Voltage, U (V)	B	17	20	23
Travel speed, v (mm/min)	C	300	400	500

Table 3 shows 17 trial runs of welding beads designed by the Box-Behnken design, which were used to develop the regression models. In addition, four extra runs (from 18 to 21)

were used to evaluate the accuracy of the developed models. In each trial run, a single welding bead was produced by the robotic GMAW system with a length of 120 mm (Figure 1b). The bead width (*BW*) and the bead height (*BH*) of a welding bead were measured at five positions in the steady region of the welding bead by using a digital caliper, and then the average value was taken, as presented in Table 3.

Table 3. Experimental design matrix and experimental results.

Run	Input variables			Response	
	A: <i>I</i> (A)	B: <i>U</i> (V)	C: <i>v</i> (mm/min)	<i>BW</i> (mm)	<i>BH</i> (mm)
1	100	17	400	3.79	3.01
2	140	17	400	4.03	3.98
3	100	23	400	5.08	2.49
4	140	23	400	5.41	3.46
5	100	20	300	4.96	3.29
6	140	20	300	5.42	4.22
7	100	20	500	4.19	2.02
8	140	20	500	4.53	3.14
9	120	17	300	4.31	4.21
10	120	23	300	6.02	3.66
11	120	17	500	3.81	3.12
12	120	23	500	5.21	2.62
13	120	20	400	4.97	3.17
14	120	20	400	5.00	3.28
15	120	20	400	4.97	3.30
16	120	20	400	4.87	3.22
17	120	20	400	5.01	3.20
18	110	18	350	4.54	3.38
19	130	22	350	5.46	3.53
20	110	18	400	4.42	3.28
21	130	22	450	5.13	2.96

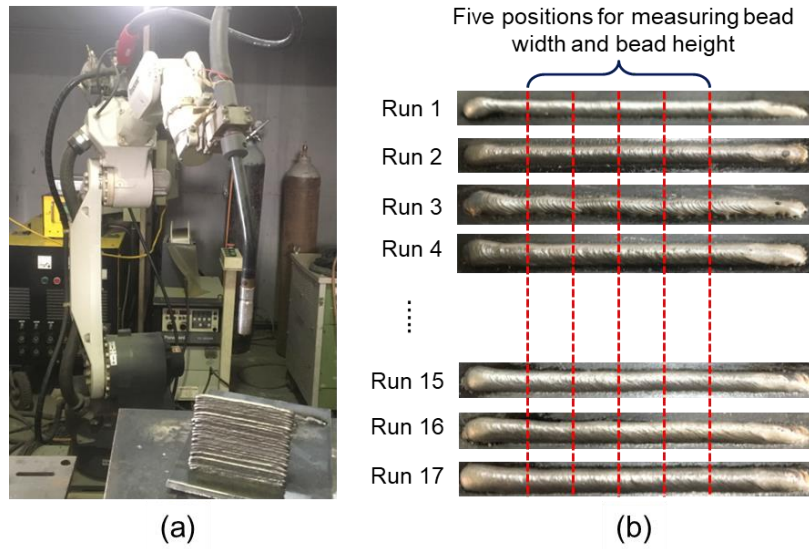


Figure 1. (a) The robotic GMAW system (Panasonic TA1400) and (b) 17 trial runs of single welding beads used for developing the regression models.

3. RESULTS AND DISCUSSION

3.1. Developing the predictive models

In the current study, the second order regression equation was adopted to develop the predictive models of bead width, bead height, eq. (1):

$$Y = b_0 + b_1I + b_2U + b_3v + b_{12}IU + b_{13}Iv + b_{23}Uv + b_{11}I^2 + b_{22}U^2 + b_{33}v^2 \quad (1)$$

where Y is the responses – i.e. the bead width BW (mm) or the bead height BH (mm), b_0 is the average of the response; b_i , b_{ii} and b_{ij} ($i, j = 1, 2, 3$ and $i \neq j$) are the coefficients, which depend on their main effects and interaction effects of the parameters on the responses, I is the welding current (A), U is the voltage (V), and v is the travel speed of the welding torch (mm/min). In this work, the coefficients were estimated by using the Design Expert 11 software. The full predictive models in terms of actual factors for the bead width and the bead height are shown in eq. (2) and eq. (3), respectively:

$$BW \text{ (mm)} = - 16.190 + 0.143I + 1.027U + 0.508 \times 10^{-3}v + 0.375 \times 10^{-3}IU - 0.016 \times 10^{-3}Iv - 0.263 \times 10^{-3}Uv - 0.567 \times 10^{-3}I^2 - 0.018U^2 + 3.67 \times 10^{-6}v^2 \quad (2)$$

$$BH \text{ (mm)} = 7.575 + 0.085I - 0.623U - 0.014v + 8.33 \times 10^{-6}IU + 0.024 \times 10^{-3}Iv + 0.048 \times 10^{-3}Uv - 0.292 \times 10^{-3}I^2 + 0.013U^2 + 5.223 \times 10^{-6}v^2 \quad (3)$$

In eq. (2) and eq. (3), the unit of the welding current I , the voltage U , and the travel speed v is “A”, “V”, and “mm/min”, respectively.

3.2. Analysis of regression models

The accuracy of the developed models was evaluated by using the analysis of variance (ANOVA) method. The results of ANOVA for the regression models of the bead width and the bead height were presented in Tables 4 and 5, respectively.

For the model of the bead width, as shown in eq. (2) and Table 4, the F-value of 78.06 indicates that the model is significant. There is only a 0.01% chance that the F-value could be large due to noise. The p-values lower than 0.05 indicate that the model terms are significant, whereas the p-values greater than 0.10 indicate the model terms are not significant. In this case, the terms {A, B, C, A² and B²} are significant terms of the developed model. The R² of 0.9901 indicates a high correlation between the experimental and the predicted values. The Predicted R² of 0.8726 is in reasonable agreement with the Adjusted R² of 0.9774. The Adeq. Precision represents the ratio of signal-to-noise. A value of this ratio greater than 4 is usually desirable. Herein, the Adeq. Precision of 32.85 indicates an adequate signal. Therefore, the developed model of the bead width is totally validated in the design space.

Table 4. ANOVA results for the regression model of the bead width (BW).

Source	Sum of Squares	Mean Square	F-value	p-value
Model	5.8900	0.6542	78.06	< 0.0001
A-Welding current, I	0.2339	0.2339	27.91	0.0011
B-Voltage, U	4.1700	4.1700	497.94	< 0.0001
C-Travel speed, v	1.1000	1.1000	131.56	< 0.0001
AB	0.0020	0.0020	0.2416	0.6381
AC	0.0040	0.0040	0.4736	0.5135
BC	0.0250	0.0250	2.98	0.1280
A²	0.2166	0.2166	25.84	0.0014
B²	0.1123	0.1123	13.40	0.0081
C²	0.0057	0.0057	0.6767	0.4379
R²	0.9901	Predicted R²	0.8726	
Adjusted R²	0.9774	Adeq. Precision	32.8534	

In the case of the bead height model (eq. (3) and Table 5), the F-value of 200.86 indicates that the model is significant. Only a 0.01% chance occurs that the F-value could enlarge due to noise. The terms {A, B, C, A² and B²} with the p-values lower than 0.05 are significant terms in the bead height model. The R² of 0.9961 indicates very good correlation between the experimental values and the predicted values. The Predicted R² of 0.9706 is in good agreement with the Adjusted R² of 0.9912. The Adeq. Precision of 53.02 higher than 4 indicates an adequate signal. Thus, the model can be used in the whole design space.

3.3. Effects of process parameters on the geometry of single welding beads

Fig. 2a and Fig. 2b present the perturbation of the bead width and the bead height, respectively, as functions of deviation from the reference point. In Fig. 2a, it is found that the voltage and the travel speed reveal significant effects on the bead width. The bead width increases when the voltage increases from 17 (V) (at -1 level) to 23 (V) (at +1 level), whereas

the bead width decreases when the travel speed increases from 300 (mm/min) (at -1 level) to 500 (mm/min) (at +1 level). Moreover, the bead width gradually increases when the welding current increases up to a certain value, and then it starts decreasing.

Table 5. ANOVA results for the regression model of the bead height (BH).

Source	Sum of Squares	Mean Square	F-value	p-value
Model	5.1800	0.5752	200.86	< 0.0001
A-Welding current, I	1.9900	1.9900	694.76	< 0.0001
B-Voltage, U	0.5513	0.5513	192.51	< 0.0001
C-Travel speed, v	2.5100	2.5100	875.13	< 0.0001
AB	0.0000	0.0000	0.0003	0.9856
AC	0.0093	0.0093	3.24	0.1149
BC	0.0008	0.0008	0.2937	0.6047
A²	0.0574	0.0574	20.05	0.0029
B²	0.0565	0.0565	19.74	0.0030
C²	0.0115	0.0115	4.01	0.0853
R²	0.9961	Predicted R²	0.9706	
Adjusted R²	0.9912	Adeq. Precision	53.0157	

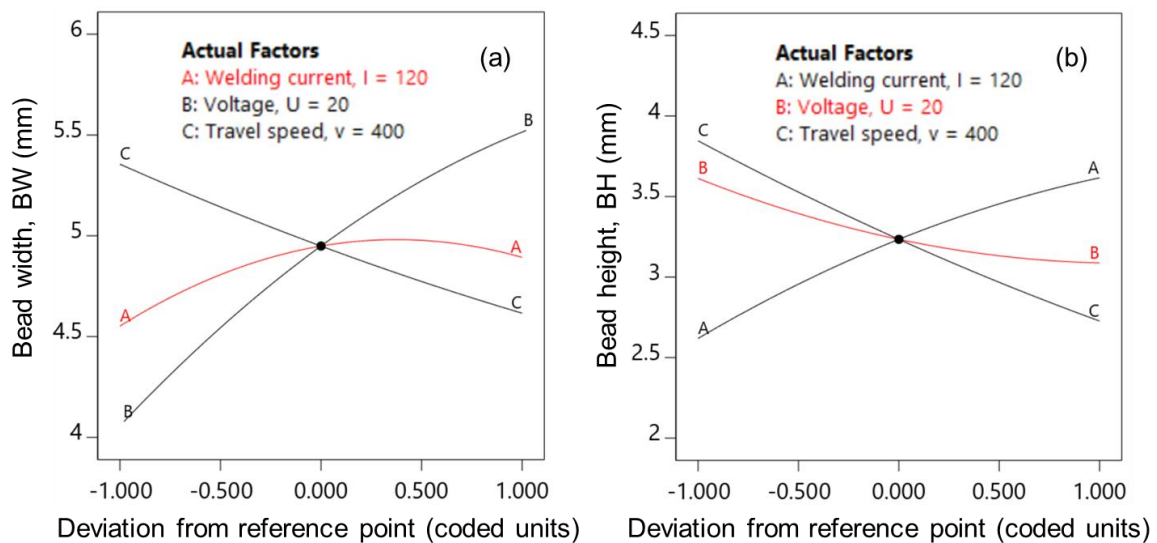


Figure 2. Main effects of process parameters on the bead width (a) and on the bead height (b).

As revealed in Fig. 2b, the travel speed and the welding current have notable effects on the bead height. An increase in the welding current from 100 (A) (at -1 level) to 140 (A) (at +1 level) leads to an augmentation in the bead height. On the other hand, the bead height decreases when the travel speed and the voltage increase in the design space.

Fig. 3 shows the interaction effects of process parameters on the bead width. It is also observed that the bead width increases with an increase in the voltage for all values of the welding current (Fig. 3a) and for all values of the travel speed (Fig. 3c). On the other hand, the increase in the travel speed also leads to a decrease in the bead width for all values of the voltage and for all values of the welding current. The bead width slightly increases with an increase in the welding current for all values of the voltage and the travel speed (Fig. 3a and Fig. 3b).

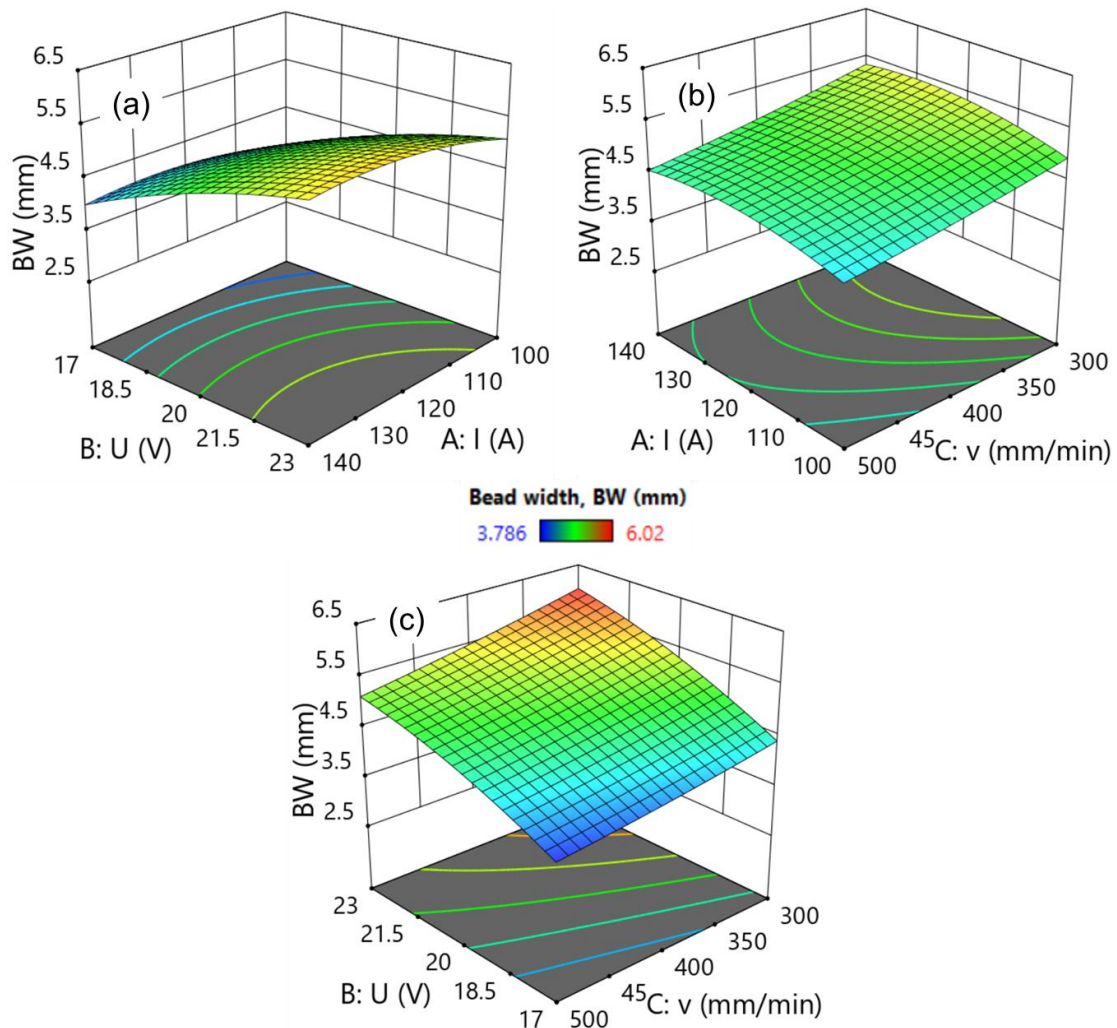


Figure 3. Interaction effects of process parameters on the bead width: (a) I and U on BW , (b) I and v on BW , and (c) U and v on BW .

The interaction effects of process parameters on the bead height were also presented in Fig. 4. It is found that the bead height increases with an increase in the current from 100 (A) to 140 (A) for all values of the voltage (Fig. 4a) and for all values of the travel speed (Fig. 4b). On the other hand, the bead height decreases with an increase in the travel speed for all

values of the welding current (Fig. 4b) and for all values of the voltage (Fig. 4c). The increase in the voltage leads to a gradual decrease in the bead height for all values of the welding current (Fig. 4a) and for all values of the travel speed (Fig. 4c). At the lowest value of the voltage and the travel speed, and at the highest value of the welding current, the bead height reaches the maximal value.

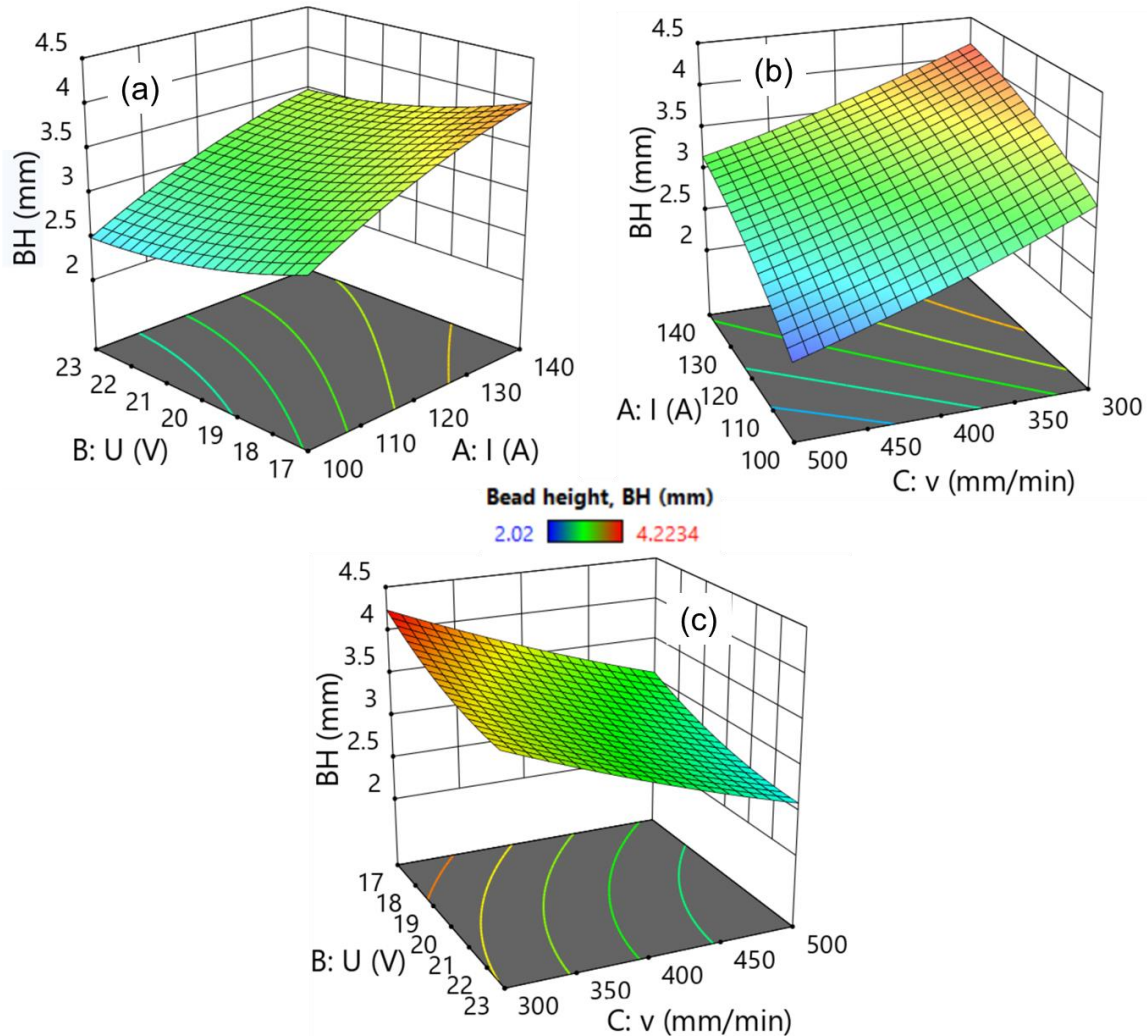


Figure 4. Interaction effects of process parameters on the bead height: (a) I and U on BH , (b) I and v on BH , and (c) U and v on BH .

The effects of the parameters on the geometry of welding beads can be explained by the following reasons: when the voltage increases, the arc length and the spreading of the arc increase too [21,22]. As a result, the bead width increases, and the bead height decreases. An excessive increase in the voltage can also cause flat welding beads. The bead width and the bead height decrease when the travel speed increases. This is due to the fact that the quantity of deposited materials per length unit and the heat input also decrease with an increase in the travel speed. Thereby, both the bead width and bead height decrease. In the GMAW process, the increase in the welding current leads to an augmentation in the wire feed speed. Namely, the rate of deposited material increases. Thus, the size of welding pool, the bead width, and the bead height increase. However, the bead width only increases up to a certain value of the

welding current and then decreases. After that, an extra deposited material does not have significant effects on the bead width, and the bead width remains almost constant or slightly decreases [21].

3.4. Validation of the regression models

In order to validate the accuracy of the regression models, the data of four extra runs (from 18 to 21 given in Table 3) was also used. The error between a predicted value (*PV*) and an experimental value (*EV*) was calculated by eq. (4):

$$Error (\%) = 100\%*(PV - EV)/EV \tag{4}$$

It is found that the errors in the percentage for the bead width (*BW*) and the bead height (*BH*) lie within the ranges of -3.28% to 3.26%, and of -2.96% to 4.10%, respectively. The small errors lower than 5% indicate that the regression models are adequate and can be used for optimizing process parameters, which would give a desirable geometry and quality of welding beads for the build of thin-walled components.

Table 6. Comparison of the experimental and the predicted values.

No.	Bead width, <i>BW</i>			Bead height, <i>BH</i>		
	<i>PV</i>	<i>EV</i>	<i>Error (%)</i>	<i>PV</i>	<i>EV</i>	<i>Error (%)</i>
18	4.44	4.54	-2.30	3.49	3.38	3.33
19	5.64	5.46	3.26	3.61	3.53	2.17
20	4.27	4.42	-3.28	3.18	3.28	-2.96
21	5.20	5.13	1.33	3.08	2.96	4.10

3.5. Optimization of the process parameters for the build of SS308L walls

Based on the developed models, the optimal process parameters can be predicted. In the WAAM process of thin walls, the bead width and the bead height of single welding beads are expected to be maximum, while the heat input (*HI*) determined by the formula $HI = 60*\eta*U*I/v$ (J/mm), where η is the coefficient of thermal efficiency and $\eta = 0.8$ for the GMAW process [23], *U* in (V), *I* in (A), and *v* in (mm/min), should be minimum. This ensures the process stability and reducing the distortion and residual stresses of the built walls [12,24,25]. Therefore, the problem of optimizing the process parameters was expressed as follows:

Find [*I*, *U*, *v*] to maximize *BW*, maximize *BH*, and minimize *HI*.

Subject to: $100 \leq I \leq 140$ (A); $17 \leq U \leq 23$ (V); $300 \leq v \leq 500$ (mm/min).

This problem was solved by using the optimization module in the Design Expert 11 software. The optimal process parameters were calculated as: *I* = 122 (A), *U* = 20 (V) and *v* = 368 (mm/min). As shown in Fig. 5, three single welding beads built by the optimized process

parameters are nearly identical. They are continuous, smooth, regular and without major defects. The average bead width and bead height are 4.95 (mm) and 3.32 (mm), respectively.



Figure 5. Three welding beads built with the optimized process parameters.

Fig. 6 shows a SS308L wall built by the GMAW-AM with the above optimized process parameters. The wall was built by using the same deposition direction strategy [26]. It is found that the width of the wall is stable. On the other hand, the height of the wall decreases from the right to the left. This phenomenon is commonly observed in the case of building thin-walled components by the same deposition direction strategy in WAAM [26].

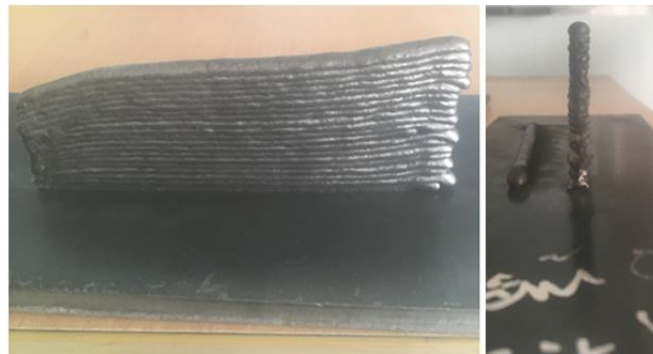


Figure 6. The GMAW-AM SS308L wall built with the optimized process parameters.

4. CONCLUSIONS

This paper aims at developing the predictive models for the bead width and the bead height in the WAAM process of SS308L components. For this purpose, a series of experimental runs were performed according to the Box-Behnken design method. The value range of the process parameters was chosen based on the recommendation of the wire manufacturer and verified by several trial runs. The regression models were developed by using the response surface methodology (RSM), and their accuracy was assessed by the analysis of variance (ANOVA). The results indicate that the regression models present a high accuracy and can be efficiently used to analyze the effects of process parameters on the welding bead geometry, and to predict the desirable bead width and bead height in the whole design space. From the developed models, the optimized process parameters, including a welding current of 122 (A), a voltage of 20 (V) and a travel speed of 368 (mm/min) were determined for the build of SS308L walls. The models developed in this study are only used to predict the optimal process parameters in the GMAW-AM of SS308L. However, the same workflow can be applied to predict the geometry of single welding beads in WAAM of other metals. In the future works, the microstructure and mechanical properties of GMAW-AM SS308L components will be investigated to confirm their adequacy for real applications.

ACKNOWLEDGMENT

This research is funded by Vietnam National Foundation for Science and Technology Development (NAFOSTED) under grant number 107.99-2019.18.

REFERENCES

- [1]. N. Guo, M. Leu, Additive manufacturing: technology, applications and research needs, *Front. Mech. Eng.*, 8 (2013) 215–243. <https://doi.org/10.1007/s11465-013-0248-8>
- [2]. V.T. Le, H. Paris, G. Mandil, Environmental impact assessment of an innovative strategy based on an additive and subtractive manufacturing combination, *J. Clean. Prod.*, 164 (2017) 508–523. <https://doi.org/10.1016/j.jclepro.2017.06.204>
- [3]. V.T. Le, H. Paris, A life cycle assessment-based approach for evaluating the influence of total build height and batch size on the environmental performance of electron beam melting, *Int. J. Adv. Manuf. Technol.*, 98 (2018) 275–288. <https://doi.org/10.1007/s00170-018-2264-7>
- [4]. K.S. Derekar, A review of wire arc additive manufacturing and advances in wire arc additive manufacturing of aluminium, *Mater. Sci. Technol.*, 34 (2018) 895–916. <https://doi.org/10.1080/02670836.2018.1455012>
- [5]. D. Ding, Z. Pan, D. Cuiuri, H. Li, Wire-feed additive manufacturing of metal components: technologies, developments and future interests, *Int. J. Adv. Manuf. Technol.*, 81 (2015) 465–481. <https://doi.org/10.1007/s00170-015-7077-3>
- [6]. S.W. Williams, F. Martina, A.C. Addison, J. Ding, G. Pardal, P. Colegrove, *Wire + Arc Additive Manufacturing*, *Mater. Sci. Technol.* 32 (2016) 641–647. <https://doi.org/10.1179/1743284715Y.0000000073>
- [7]. J. Xiong, Y. Li, R. Li, Z. Yin, Influences of process parameters on surface roughness of multi-layer single-pass thin-walled parts in GMAW-based additive manufacturing, *J. Mater. Process. Technol.*, 252 (2018) 128–136. <https://doi.org/10.1016/j.jmatprotec.2017.09.020>
- [8]. Z. Zhang, C. Sun, X. Xu, L. Liu, Surface quality and forming characteristics of thin-wall aluminium alloy parts manufactured by laser assisted MIG arc additive manufacturing, *Int. J. Light. Mater. Manuf.*, 1 (2018) 89–95. <https://doi.org/10.1016/j.ijlmm.2018.03.005>
- [9]. S. Jindal, R. Chhibber, N.P. Mehta, Effect of welding parameters on bead profile, microhardness and H₂ content in submerged arc welding of high-strength low-alloy steel, *Proc. Inst. Mech. Eng. Part B J. Eng. Manuf.* 228 (2014) 82–94. <https://doi.org/10.1177/0954405413495846>
- [10]. G. Magudeeswaran, S.R. Nair, L. Sundar, N. Harikannan, Optimization of process parameters of the activated tungsten inert gas welding for aspect ratio of UNS S32205 duplex stainless steel welds, *Def. Technol.*, 10 (2014) 251–260. <https://doi.org/10.1016/j.dt.2014.06.006>
- [11]. S. Srivastava, R.K. Garg, Process parameter optimization of gas metal arc welding on IS:2062 mild steel using response surface methodology, *J. Manuf. Process.*, 25 (2017) 296–305. <https://doi.org/10.1016/j.jmapro.2016.12.016>
- [12]. J. Xiong, G. Zhang, W. Zhang, Forming appearance analysis in multi-layer single-pass GMAW-based additive manufacturing, *Int. J. Adv. Manuf. Technol.*, 80 (2015) 1767–1776. <https://doi.org/10.1007/s00170-015-7112-4>
- [13]. X. Lu, Y.F. Zhou, X.L. Xing, L.Y. Shao, Q.X. Yang, S.Y. Gao, Open-source wire and arc additive manufacturing system: formability, microstructures, and mechanical properties, *Int. J. Adv. Manuf. Technol.*, 93 (2017) 2145–2154. <https://doi.org/10.1007/s00170-017-0636-z>
- [14]. H. Takagi, H. Sasahara, T. Abe, H. Sannomiya, S. Nishiyama, S. Ohta, K. Nakamura, Material-property evaluation of magnesium alloys fabricated using wire-and-arc-based additive manufacturing, *Addit. Manuf.*, 24 (2018) 498–507. <https://doi.org/10.1016/j.addma.2018.10.026>
- [15]. M. Dinovitzer, X. Chen, J. Laliberte, X. Huang, H. Frei, Effect of wire and arc additive manufacturing (WAAM) process parameters on bead geometry and microstructure, *Addit. Manuf.*, 26 (2019) 138–146. <https://doi.org/10.1016/j.addma.2018.12.013>
- [16]. M. Rafieezad, M. Ghaffari, A. Vahedi Nemani, A. Nasiri, Microstructural evolution and mechanical properties of a low-carbon low-alloy steel produced by wire arc additive manufacturing,

- Int. J. Adv. Manuf. Technol., 105 (2019) 2121–2134. <https://doi.org/10.1007/s00170-019-04393-8>
- [17]. V.T. Le, A preliminary study on gas metal arc welding-based additive manufacturing of metal parts, *Sci. Technol. Dev. J.* 23 (2020) 422–429. <https://doi.org/10.32508/stdj.v23i1.1714>
- [18]. X. Chen, J. Li, X. Cheng, B. He, H. Wang, Z. Huang, Microstructure and mechanical properties of the austenitic stainless steel 316L fabricated by gas metal arc additive manufacturing, *Mater. Sci. Eng. A.*, 703 (2017) 567–577. <https://doi.org/10.1016/j.msea.2017.05.024>
- [19]. C. V. Haden, G. Zeng, F.M. Carter, C. Ruhl, B.A. Krick, D.G. Harlow, Wire and arc additive manufactured steel: Tensile and wear properties, *Addit. Manuf.*, 16 (2017) 115–123. <https://doi.org/10.1016/j.addma.2017.05.010>
- [20]. W. Wu, J. Xue, Z. Zhang, P. Yao, Comparative study of 316L depositions by two welding current processes, *Mater. Manuf. Process.*, 34 (2019) 1502-1508. <https://doi.org/10.1080/10426914.2019.1643473>
- [21]. V. Gunaraj, N. Murugan, Application of response surface methodology for predicting weld bead quality in submerged arc welding of pipes, *J. Mater. Process. Technol.*, 88 (1999) 266–275. [https://doi.org/10.1016/S0924-0136\(98\)00405-1](https://doi.org/10.1016/S0924-0136(98)00405-1)
- [22]. S. Jindal, R. Chhibber, N.P. Mehta, Effect of welding parameters on bead profile, microhardness and H₂ content in submerged arc welding of high-strength low-alloy steel, *Proc. Inst. Mech. Eng. Part B J. Eng. Manuf.* 228 (2014) 82–94. <https://doi.org/10.1177/0954405413495846>
- [23]. I. Jurić, I. Garašić, M. Bušić, Z. Kožuh, Influence of Shielding Gas Composition on Structure and Mechanical Properties of Wire and Arc Additive Manufactured Inconel 625, *Jom.*, 71 (2019) 703–708. <https://doi.org/10.1007/s11837-018-3151-2>
- [24]. F. Youheng, W. Guilan, Z. Haiou, L. Liye, Optimization of surface appearance for wire and arc additive manufacturing of Bainite steel, *Int. J. Adv. Manuf. Technol.*, 91 (2017) 301–313. <https://doi.org/10.1007/s00170-016-9621-1>
- [25]. D. Yang, G. Wang, G. Zhang, Thermal analysis for single-pass multi-layer GMAW based additive manufacturing using infrared thermography, *J. Mater. Process. Technol.*, 244 (2017) 215–224. <https://doi.org/10.1016/j.jmatprotec.2017.01.024>
- [26]. J. Xiong, Z. Yin, W. Zhang, Forming appearance control of arc striking and extinguishing area in multi-layer single-pass GMAW-based additive manufacturing, *Int. J. Adv. Manuf. Technol.*, 87 (2016) 579–586. <https://doi.org/10.1007/s00170-016-8543-2>